Title: Synaptic plasticity at intrathalamic connections via CaV3.3 T-type Ca2+ channels and GluN2B-containing NMDA receptors.

Authors: Astori S, Lüthi A

Journal: The Journal of neuroscience

Year: 2013 Jan 9

Volume: 33

Issue: 2

Pages: 624-30

DOI: 10.1523/JNEUROSCI.3185-12.2013

Brief Communication

Synaptic plasticity at intrathalamic connections via $Ca_V3.3$ T-type Ca^{2+} channels and GluN2B-containing NMDA receptors

Abbreviated Title: Plasticity at thalamoreticular synapses

Simone Astori[a1] & Anita Lüthi[a1]

[a]Department of Fundamental Neurosciences, University of Lausanne, Rue du Bugnon 9, CH-1005 Lausanne, Switzerland.

[1] Corresponding author:

Department of Fundamental Neurosciences,
University of Lausanne,
Bugnon 9
CH-1005 Lausanne
Phone: +41 21 692 5294
Fax: +41 21 692 5105
E-mail: simone.astori@unil.ch; anita.luthi@unil.ch

Number of pages:	21
Number of figures:	4
Number of tables:	0
Number of words in abstract:	77
Number of words in introduction:	309
Number of words in discussion:	566
Total number of words:	4765

The authors declare no competing financial interests.

Acknowledgements

We thank all laboratory members for critical reading of the manuscript and Dr. Georg Köhr for helpful comments and discussion. We are grateful to Dr. Ceri Davis for acting as a GlaxoSmithKline referent. This work was supported by the Swiss National Science Foundation (Ambizione grant to S.A. and nr. 129810 to A.L.) and by the Synapsis Foundation.

The T-type Ca^{2+} channels encoded by the *Ca_V3* genes are well-established electrogenic drivers for burst discharge. Here, using $Ca_V3.3^{-/-}$ mice we found that $Ca_V3.3$ channels trigger synaptic plasticity in reticular thalamic neurons. Burst discharge via $Ca_V3.3$ channels induced long-term potentiation at thalamoreticular inputs when co-activated with GluN2B-containing NMDA receptors, which are the dominant subtype at these synapses. Notably, oscillatory burst discharge of reticular neurons is typical for sleep-related rhythms, suggesting that sleep contributes to strengthening intrathalamic circuits.

Introduction

T-type Ca^{2+} channels generate low-threshold discharges essential for neuronal rhythmogenesis (Huguenard, 1996), and, additionally, are involved in a variety of physiological and pathological conditions, such as sensory transmission, neurotransmitter release, neuronal development and pain (Cueni et al., 2009). The three T-channel subtypes ($Ca_V3.1$-3) show different expression patterns and distinct biophysical and pharmacological properties (Talley et al., 1999; Perez-Reyes, 2003). Whether such diversity accounts for specific roles has not yet been fully addressed, mainly because the pharmacological tools available are not subtype-specific, and, additionally, exert non-selective actions on other Ca^{2+} channels (Perez-Reyes, 2003).

A role for T-channels in promoting synaptic plasticity has been suggested by several studies, e.g. in cortex and hippocampus (Thomas et al., 1998; Schmidt-Hieber et al., 2004; Nevian and Sakmann, 2006; Lanté et al., 2011). Here, we made use of a mutant mouse lacking the *$Ca_V3.3$* gene (Astori et al., 2011) to demonstrate the involvement of $Ca_V3.3$ channels in a novel form of intrathalamic plasticity. In the *nucleus Reticularis thalami* (nRt), a component of the thalamocortical system, $Ca_V3.3$ channels represent a potent source for dendritic $[Ca^{2+}]_i$ elevations (Cueni et al., 2008; Astori et al., 2011). Moreover, NMDA receptors (NMDARs), another Ca^{2+} source and trigger for synaptic plasticity, are expressed at both thalamoreticular and corticoreticular synapses (Gentet and Ulrich, 2003, 2004), but their proplastic role has not been explored.

We first investigated NMDAR-signaling at thalamic inputs by means of patch-clamp electrophysiology on acute slices *ex vivo*, and found that GluN2B-containing NMDARs (GluN2B-NMDARs) represent the major NMDAR subtype at both developing and mature synapses. GluN2B-NMDAR activation associated with oscillatory low-threshold spiking induced long-term potentiation of thalamoreticular synapses. Potentiation was lacking in $Ca_V3.3^{-/-}$ mice, in which burst discharge is

largely suppressed. Notably, oscillatory bursting resembles physiological activity patterns typical for NREM sleep (Steriade, 2006), suggesting that $Ca_V3.3$ channels and GluN2B-NMDARs may contribute to strengthen intrathalamic circuits and regulate sleep waves.

Materials and Methods

Electrophysiological recordings and analyses. All procedures were approved by the Veterinary Office of Canton de Vaud. Typically, acute horizontal brain slices (300 μm-thick) were prepared as previously described (Cueni et al., 2008) from 3-4 week-old (wk-old) C57Bl/6J and $Ca_V3.3^{-/-}$ mice of either sex. In a subset of experiments, 2 wk-old or 7-8 wk-old animals were used. For comparative characterization of cortical vs. thalamic inputs, thalamocortical slices (Agmon and Connors, 1991) were prepared. Animals were maintained under 12:12h light/dark schedule (lights on at 7AM), and slices were prepared between 11AM and 12AM. The $Ca_V3.3^{-/-}$ mouse line, originally obtained from GlaxoSmithKline, was maintained in the institute's animal facility and genotyped as previously described (Astori et al., 2011).

Slices were constantly superfused with oxygenated artificial CFS (ACSF) containing (in mM): 125 NaCl, 25 $NaHCO_3$, 2.5 KCl, 1.25 NaH_2PO_4, 1.2 $MgCl_2$, 2 $CaCl_2$, 25 glucose, 1.7 L(+)-ascorbic acid, 0.1 picrotoxin, 0.01 glycine. Recordings were performed at 30°-32°C. Visually identified nRt neurons were whole-cell patched with borosilicate glass pipettes (TW150F-4, WPI). Typically, pipettes (3-5 MΩ) were filled with (in mM): 140 $KMeSO_4$, 10 KCl, 10 HEPES, 0.1 EGTA, 4 Mg-ATP, 0.2 Na-GTP, 10 phosphocreatine (290-300 mOsm, pH 7.25). For some recordings, 0.5 mM N-(2,6-Dimethylphenylcarbamoylmethyl)-triethylammonium-chloride (QX-314) or 2 mM 1,2-bis(o-aminophenoxy)ethane-*N,N,N′,N′*-tetraacetic acid (BAPTA) were included in the pipette. A liquid junction potential of -10 mV was taken into account. For NMDA-EPSCs, pipettes (3-4 MΩ) were

filled with (in mM): 127 CsGluconate, 10 HEPES, 2 BAPTA, 6 $MgCl_2$, 2 Mg-ATP, 0.2 Na-GTP, 10 phosphocreatine (290-300 mOsm, pH 7.25), 2.5 QX-314. A liquid junction potential of -8 mV was corrected for. In horizontal slices, EPSCs were evoked every 30 s by stimulation in the internal capsule with an ACSF-filled electrode. In thalamocortical slices, the electrode was placed in cortical layer 6 or in the striatum adjacent to the cortex. Paired-pulse ratio (PPR, 50 ms interval) was measured from average responses (≥4 sweeps) as peak2/peak1.

For NMDA/AMPA ratios and NMDAR pharmacology, EPSCs were first evoked at -70 mV. Subsequently, cells were depolarized to +40 mV, and DNQX (40 μM) was bath-applied to block AMPAR-mediated transmission. NMDA-EPSC amplitude was measured as mean of 1 ms around the absolute peak of the average of 4 sweeps. This value was divided by the average EPSC peak at -70 mV to evaluate NMDA/AMPA ratios. NMDAR-GluN2-directed blockers were bath-applied for >4 min.

For plasticity experiments, baseline EPSCs were recorded for 10 min at -70 mV. Subsequently, cells were hyperpolarized to -80/-90 mV in current-clamp with DC injections, to ensure complete T-channel recovery from inactivation. Induction protocols consisted of sinusoidal current injections for 3 or 6 min (1 Hz, 0.15-0.3 nA maximal amplitude) to elicit low-threshold bursting, accompanied by paired or unpaired synaptic stimulation, as stated. Given the variability of burst onset and duration, it was not possible to define a fixed timing for the presynaptic stimulation relative to postsynaptic discharge. For series with 3 min or 6 min paired oscillations, we measured *post hoc* the time interval (Δt) between the first action potential and stimulation onset at three time points (beginning, middle, and end of the oscillation) to obtain a mean Δt for each cell. Mean Δt values ranged between -73/+76 ms (on average 23 ± 10 ms, n = 14). No correlation was found between Δt values and extent of plasticity induced (Pearson's correlation coefficient: r = 0.24, p = 0.41). For unpaired induction

protocols, stimulation was delivered at the trough of the current injection (Δt = -400/-450 ms). To test for tonic firing-induced plasticity, membrane potential was adjusted to ~-60 mV, and 200 ms-long squared pulses of 0.5/0.6 nA were provided at 1 Hz with synaptic stimulation.

After induction, EPSC recording was resumed for 30 min. Change in synaptic efficacy was calculated by comparing average EPSCs during the last 10 min of recording with baseline average EPSCs. Series resistance (R_s) was monitored throughout recordings by brief voltage-pulses, and data were rejected for R_s changes >25%. Data were acquired through a Digidata1320 digitizer. Signals were amplified through a Multiclamp700B amplifier (Molecular Devices), sampled at 20 kHz and filtered at 10 kHz using Clampex10 (Molecular Devices). Clampfit10 (Molecular Devices) and Igor5 Pro (WaveMetrics) were used for data analysis.

Data are presented as mean ± SEM. Paired or unpaired Student's *t*-test was used as appropriate with significance accepted for $p < 0.05$. For comparison between age groups, one-way ANOVA was used followed by *post hoc* Student's *t*-test.

Chemicals. All standard salts and chemicals were purchased from Sigma-Aldrich, except the following: $KMeSO_4$ (ICN Biomedicals), L(+)-ascorbic acid (VWR Prolabo), picrotoxin and DNQX (Abcam), QX-314 and PPDA (Tocris). NVP-AAM077 was provided by Novartis Pharma. CP101,606 was provided by Pfizer Pharmaceuticals.

Results

GluN2B-NMDAR-mediated transmission at thalamoreticular synapses

Gabaergic nRt cells receive glutamatergic inputs from thalamocortical cells and from layer 6 pyramidal cells. We first verified in the thalamocortical slice preparation that these two classes of inputs can be separated based on different short-term plasticity (Fig. 1). When stimulated in layer 6,

corticoreticular responses consisted of long-latency facilitating EPSCs of relatively small amplitude. In contrast, antidromic stimulation of myelinated thalamic axons elicited short-latency EPSCs with larger depressant amplitudes. These findings were consistent with previous literature (Golshani et al., 2001; Gentet and Ulrich, 2003, 2004), and allowed identification of thalamoreticular depressant EPSCs when stimulating the internal capsule in horizontal slices in subsequent recordings.

We examined basic properties of NMDAR-transmission at thalamoreticular synapses. In 3-4 wk-old mice, a significant NMDAR component was present at resting potential, as revealed by bath-application of 100 μM DL-APV, which accelerated decay kinetics of EPSCs at -70 mV (decay slope: 223 ± 50 pA/ms vs. 290 ± 60 pA/ms, $n = 9$, $p < 0.01$; Fig 2*A*). NMDAR blockade affected neither peak amplitude nor paired-pulse ratio (PPR) of EPSCs (Fig. 2*B*), indicating that presynaptic NMDARs are unlikely to modulate basal transmission. In addition, these findings ensured that the pharmacological profile of postsynaptic NMDARs could be assessed without interfering with glutamate release. The NMDA/AMPA ratio significantly decreased after the second postnatal week from 0.42 ± 0.06 ($n = 9$) to 0.27 ± 0.04 ($n = 14$), and remained stable afterwards at least until 7-8 weeks (0.26 ± 0.03, $n = 10$, $p < 0.05$) (Fig. 2*C*), indicating synaptic maturation, as found in other brain structures (Liu et al., 1996; Brill and Huguenard, 2008).

We next examined NMDAR subunit composition. GluN2 subunit expression is typically developmentally regulated such that GluN2B predominates at birth, while GluN2A expression starts in the first postnatal week and increases with maturation in most brain regions (Monyer et al., 1994). Surprisingly, decay times of NMDA-EPSCs remained constant at the three developmental stages examined ($p > 0.05$) (Fig. 2*D*), suggesting no major changes in GluN2 content. Indeed, the pharmacological profile of NMDA-EPSCs was comparable at all stages ($p > 0.05$) (Fig. 2*E*). The GluN2A-preferring antagonist NVP-AAM077 (NVP, 50 nM) (Auberson et al., 2002; Berberich et

al., 2005) reduced NMDA-EPSCs in 2 wk-old and 3-4 wk-old mice to a similar extent (2 wk-old: 71.6 ± 3.6% of control, $n = 6$, $p < 0.05$ drug vs. control; 3-4 wk-old: 76.6 ± 4.1%, $n = 8$, $p < 0.05$). Subsequent application of the GluN2B-specific blocker CP101,606 (CP, 10 μM)(Mott et al., 1998) provoked a further reduction to 12.9 ± 2.2% and 22.7 ± 3.4%, respectively ($p < 0.01$ in both cases). Similarly, NVP had a minor effect compared to CP in 7-8 wk-old mice (NVP: 86.5 ± 7.1%, NVP+CP: 24.8 ± 4.1%, $n = 6$, $p = 0.36$ and $p < 0.01$, respectively). In 3-4 wk-old mice, we quantified the relative contribution of GluN2-subtypes to NMDAR transmission. When CP was applied in the absence of NVP, to avoid unspecific actions of NVP on GluN2B-NMDARs (Berberich et al., 2005; Longordo et al., 2009), NMDA-EPSCs were reduced to 34.1 ± 3.6% of control (3-4 wk-old, $n = 8$, $p = 0.07$ compared to NVP+CP) (Fig. 2*F*). Moreover, NMDA-EPSCs were sensitive to the GluN2C/D-preferring antagonist PPDA (500 nM) (Harney et al., 2008), which reduced control responses to 71.6 ± 6.6% ($n = 7$, $p < 0.05$). Subsequent application of NVP and CP further reduced NMDA-EPSCs to 57.6 ± 4.8% ($p < 0.05$) and 13.3 ± 3.2% ($p < 0.01$), respectively (Fig. 2*F*). Notably, PPDA, similarly to DL-APV, slightly but significantly accelerated decay kinetics of EPSCs at -70 mV (decay slope: 155 ± 47 pA/ms vs. 201 ± 56 pA/ms, $n = 8$, $p < 0.05$; Fig 2*G*), whereas CP had no effect (185 ± 42 pA/ms vs. 176 ± 26 pA/ms, $n = 6$, $p > 0.05$; Fig 2*H*). Thus, in addition to GluN2B- and GluN2A-NMDARs, GluN2C/D-NMDARs are present at thalamoreticular synapses and are likely to be recruited during glutamatergic transmission at resting membrane potential.

In summary, our data suggest a complex composition of NMDARs at thalamoreticular synapses. Although a contribution of triheteromeric NMDARs (Rauner and Köhr, 2011) with undefined sensitivity to the antagonists employed here cannot be excluded, our results indicate that

GluN2B-containing NMDARs remain the predominant subtype throughout development and adulthood.

Burst-induced, NMDAR-dependent plasticity in nRt cells

We hypothesized that rhythmic discharge occurring during sleep waves, which relies on coincident activation of neurons in the thalamocortical system, could be conducive for intrathalamic plasticity. To mimic these rhythms in acute slices *ex vivo*, after recording baseline EPSCs, we elicited repetitive low-threshold discharge in hyperpolarized nRt cells by sinusoidal current injections in the δ frequency range (1 Hz) (see Materials and Methods). Pairing synaptic inputs with burst discharge resulted in subsequent EPSC long-term potentiation (Fig. 3*A*,*B*). The duration of the pairing protocol (3 min vs. 6 min) seemed to affect the time course of EPSC potentiation, but had no significant effect on its final extent (38 ± 9%, $n = 7$ vs. 52 ± 18%, $n = 7$, $p > 0.05$ between groups). Lack of change in the PPR of baseline EPSCs vs. potentiated EPSCs (Fig. 3*G*) suggested a postsynaptic locus of expression. To assess the requirement of synaptic activity for plasticity induction, we elicited burst discharge alone or with temporally unpaired synaptic inputs, both of which resulted in no potentiation (Fig. 3*C,D*). Next, we asked whether pairing-induced plasticity is NMDAR-dependent. EPSC potentiation was prevented by CP (-0.7 ± 2.9%, $n = 9$, $p > 0.05$) (Fig. 3*E*), but still inducible in the presence of NVP and PPDA (36.0 ± 9.3%, $n = 10$, $p < 0.05$) (Fig. 3*F*), indicating an obligatory requirement for induction via GluN2B-NMDARs.

Requirement of $Ca_V3.3$ channels for burst-induced plasticity

Low-threshold bursts in nRt cells consist of large Ca^{2+} spikes crowned by Na^+-dependent action potentials and arranged in cycles that are sustained by SK2-channel-mediated repolarization (Cueni

et al., 2008). On the one hand, Ca^{2+} spikes alone could sufficiently depolarize nRt dendrites to relieve the Mg^{2+} block of NMDARs. On the other hand, the robust Ca^{2+} influx mediated by T-channels could be necessary to induce plasticity in synergy with GluN2B-NMDARs.

To test for the first hypothesis, we took two complementary approaches. First, we suppressed action potentials by blocking Na_V channels with intracellular QX-314 (0.5 mM). This concentration was chosen to minimize unspecific blockade of T-channels (Talbot and Sayer, 1996), while ensuring sufficient Na_V channel blockade at the subthreshold potentials reached during current injections (Fig. 4*A*, inset). Pairing-induced plasticity could still occur in this configuration (38 ± 13%, $n = 7$, $p < 0.05$) (Fig. 4*A*), although the time course of the potentiation appeared to be slower compared to control. Thus, action potential discharge is not necessary for plasticity induction. Second, we modified the induction protocol to promote tonic discharge over low-threshold bursting: we applied depolarizing squared pulses to nRt cells held at -60 mV (see Materials and Methods), which resulted in robust suprathreshold firing with negligible T-channel contribution (Cueni et al., 2008; Astori et al., 2011). No change in synaptic efficacy was induced by pairing tonic firing with synaptic stimulation (6 ± 7%, $n = 8$, $p > 0.05$) (Fig. 4*B*), indicating that repetitive action potential discharge is not sufficient to induce plasticity.

To test for the second hypothesis, we included the Ca^{2+} chelator BAPTA (2 mM) in the intracellular solution, which prevented potentiation (8.7 ± 8.8%, $n = 6$, $p > 0.05$) (Fig. 4*C*). Finally, we made use of $Ca_V3.3^{-/-}$ mice, in which nRt low-threshold bursting is largely suppressed (Astori et al., 2011). These mice displayed comparable thalamoreticular transmission to wild-type mice (NMDA/AMPA ratio: 0.31 ± 0.03, $n = 13$) and, more specifically, the same NMDAR pharmacological profile (NVP: 89.7 ± 9.6%, NVP+CP: 20.1 ± 4.2%, $n = 7$, $p = 0.6$ and $p < 0.01$, respectively). Although action potentials could be still elicited by sinusoidal oscillations, plasticity

did not occur (7.2 ± 7.7%, $n = 7$, $p > 0.05$) (Fig. 4*D*), indicating that $Ca_V3.3$ channel activation is a requirement for synaptic potentiation.

Discussion

Within thalamic regions, $Ca_V3.3$ channels are restricted to the nRt (Talley et al., 1999) and endow reticular neurons with oscillatory properties that are the cellular basis of sleep spindles (Astori et al., 2011). In the present study, we have identified a further role for $Ca_V3.3$ channels as triggers of synaptic plasticity. Repetitive bursting associated with synaptic simulation induced long-term potentiation of thalamic inputs. Potentiation required GluN2B-NMDARs and could be induced even in the absence of Na^+-action potentials, indicating that low-threshold spiking was sufficient to enable coincidence detection via NMDARs. In contrast, if postsynaptic depolarization was provided by Na^+-dependent firing without T-channel contribution, or if low-threshold bursting was suppressed by $Ca_V3.3$ deletion, no potentiation occurred.

To repetitively co-activate $Ca_V3.3$ channels and NMDARs, we applied sinusoidal current injections to nRt cells conjointly with stimulation of thalamic inputs. This paradigm mimics some of the major electrical patterns occurring *in vivo* during physiological slow-wave sleep (Crunelli et al., 2006; Steriade, 2006). In this stage of NREM sleep, the thalamocortical system displays oscillatory electrical activity in the δ frequency range (0.5-4 Hz) generated by synchronous neuronal discharge. During NREM sleep, nRt cells are hyperpolarized, and low-threshold bursting becomes the dominant discharge mode, whereas tonic discharge is detected during waking and REM (Fuentealba and Steriade, 2005). Notably, sustained tonic discharge failed to induce plasticity. The modest Ca^{2+} influx generated by high-voltage-gated Ca^{2+} channels in nRt cells during action potentials (Cueni et al., 2008; Crandall et al., 2010) is probably insufficient to trigger plasticity, despite the contribution of NMDAR-mediated Ca^{2+} signaling. An alternative explanation is that a precise timing between pre- and postsynaptic signals could be required to generate spike-timing-dependent plasticity, which is an interesting subject for future investigations. Altogether, our data provide first evidence that

thalamic centers are capable of long-term synaptic plasticity and suggest a mechanism by which intrathalamic synapses could boost sleep rhythms.

The persistence of GluN2B-NMDARs throughout development and adulthood is a remarkable feature of thalamoreticular synapses. The lack of a developmental switch in favor of GluN2A-NMDARs has been documented in only few other glutamatergic synapses, e.g. in the amygdala (Lopez de Armentia and Sah, 2003). Notably, thalamocortical neurons have already been reported to retain an immature phenotype by showing high expression of the differentiation-promoting transcription factor LEF1 (Wisniewska et al., 2010) and of HCN4 channels (Wenzel et al., 1997; Kanyshkova et al., 2009) that promote oscillatory discharge. We also found a component of NMDAR-currents that was recruited at resting potential and sensitive to the GluN2C/D-preferring blocker PPDA. This component is likely to be mediated by GluN2C-NMDARs, that are expressed in thalamic regions (Monyer et al., 1994; Wenzel et al., 1997), and our data provide functional evidence for their presence at thalamoreticular synaptic sites. The unusual composition of NMDARs in nRt might have interesting functional implications. GluN2 composition is highly susceptible to sensory experience, environmental enrichment and learning (Kopp et al., 2007). Additionally, in different brain areas, GluN2 subunit trafficking has been shown to be sensitive to sleep deprivation (Kopp et al., 2007; Longordo et al., 2009) and to be modulated by arousal and sleep-promoting agents, such as orexins and adenosine (Borgland et al., 2006; Deng et al., 2011). Whether there are factors that modify intrathalamic NMDARs or whether there are protective mechanisms that retain the juvenile phenotype is an intriguing question arising from this work that may shed novel light on thalamic function and its unusual $Ca_V3.3$-gated plasticity.

References

Agmon A, Connors BW (1991) Thalamocortical responses of mouse somatosensory (barrel) cortex in vitro. Neuroscience 41:365-379.

Astori S, Wimmer RD, Prosser HM, Corti C, Corsi M, Liaudet N, Volterra A, Franken P, Adelman JP, Lüthi A (2011) The $Ca_V3.3$ calcium channel is the major sleep spindle pacemaker in thalamus. Proc Natl Acad Sci U S A 108:13823-13828.

Auberson YP, Allgeier H, Bischoff S, Lingenhoehl K, Moretti R, Schmutz M (2002) 5-Phosphonomethylquinoxalinediones as competitive NMDA receptor antagonists with a preference for the human 1A/2A, rather than 1A/2B receptor composition. Bioorg Med Chem Lett 12:1099-1102.

Berberich S, Punnakkal P, Jensen V, Pawlak V, Seeburg PH, Hvalby O, Köhr G (2005) Lack of NMDA receptor subtype selectivity for hippocampal long-term potentiation. J Neurosci 25:6907-6910.

Borgland SL, Taha SA, Sarti F, Fields HL, Bonci A (2006) Orexin A in the VTA is critical for the induction of synaptic plasticity and behavioral sensitization to cocaine. Neuron 49:589-601.

Brill J, Huguenard JR (2008) Sequential changes in AMPA receptor targeting in the developing neocortical excitatory circuit. J Neurosci 28:13918-13928.

Crandall SR, Govindaiah G, Cox CL (2010) Low-threshold Ca^{2+} current amplifies distal dendritic signaling in thalamic reticular neurons. J Neurosci 30:15419-15429.

Crunelli V, Cope DW, Hughes SW (2006) Thalamic T-type Ca^{2+} channels and NREM sleep. Cell Calcium 40:175-190.

Cueni L, Canepari M, Adelman JP, Lüthi A (2009) Ca^{2+} signaling by T-type Ca^{2+} channels in neurons. Pflugers Arch 457:1161-1172.

Cueni L, Canepari M, Lujàn R, Emmenegger Y, Watanabe M, Bond CT, Franken P, Adelman JP, Lüthi A (2008) T-type Ca^{2+} channels, SK2 channels and SERCAs gate sleep-related oscillations in thalamic dendrites. Nat Neurosci 11:683-692.

Deng Q, Terunuma M, Fellin T, Moss SJ, Haydon PG (2011) Astrocytic activation of A1 receptors regulates the surface expression of NMDA receptors through a Src kinase dependent pathway. Glia 59:1084-1093.

Fuentealba P, Steriade M (2005) The reticular nucleus revisited: intrinsic and network properties of a thalamic pacemaker. Prog Neurobiol 75:125-141.

Gentet LJ, Ulrich D (2003) Strong, reliable and precise synaptic connections between thalamic relay cells and neurones of the nucleus reticularis in juvenile rats. J Physiol 546:801-811.

Gentet LJ, Ulrich D (2004) Electrophysiological characterization of synaptic connections between layer VI cortical cells and neurons of the nucleus reticularis thalami in juvenile rats. Eur J Neurosci 19:625-633.

Golshani P, Liu XB, Jones EG (2001) Differences in quantal amplitude reflect GluR4-subunit number at corticothalamic synapses on two populations of thalamic neurons. Proc Natl Acad Sci U S A 98:4172-4177.

Harney SC, Jane DE, Anwyl R (2008) Extrasynaptic NR2D-containing NMDARs are recruited to the synapse during LTP of NMDAR-EPSCs. J Neurosci 28:11685-11694.

Huguenard JR (1996) Low-threshold calcium currents in central nervous system neurons. Annu Rev Physiol 58:329-348.

Kanyshkova T, Pawlowski M, Meuth P, Dubé C, Bender RA, Brewster AL, Baumann A, Baram TZ, Pape HC, Budde T (2009) Postnatal expression pattern of HCN channel isoforms in thalamic neurons: relationship to maturation of thalamocortical oscillations. J Neurosci 29:8847-8857.

Kopp C, Longordo F, Lüthi A (2007) Experience-dependent changes in NMDA receptor composition at mature central synapses. Neuropharmacology 53:1-9.

Lanté F, Toledo-Salas JC, Ondrejcak T, Rowan MJ, Ulrich D (2011) Removal of synaptic Ca^{2+}-permeable AMPA receptors during sleep. J Neurosci 31:3953-3961.

Liu YB, Lio PA, Pasternak JF, Trommer BL (1996) Developmental changes in membrane properties and postsynaptic currents of granule cells in rat dentate gyrus. J Neurophysiol 76:1074-1088.

Longordo F, Kopp C, Mishina M, Lujàn R, Lüthi A (2009) NR2A at CA1 synapses is obligatory for the susceptibility of hippocampal plasticity to sleep loss. J Neurosci 29:9026-9041.

Lopez de Armentia M, Sah P (2003) Development and subunit composition of synaptic NMDA receptors in the amygdala: NR2B synapses in the adult central amygdala. J Neurosci 23:6876-6883.

Monyer H, Burnashev N, Laurie DJ, Sakmann B, Seeburg PH (1994) Developmental and regional expression in the rat brain and functional properties of four NMDA receptors. Neuron 12:529-540.

Mott DD, Doherty JJ, Zhang S, Washburn MS, Fendley MJ, Lyuboslavsky P, Traynelis SF, Dingledine R (1998) Phenylethanolamines inhibit NMDA receptors by enhancing proton inhibition. Nat Neurosci 1:659-667.

Nevian T, Sakmann B (2006) Spine Ca^{2+} signaling in spike-timing-dependent plasticity. J Neurosci 26:11001-11013.

Perez-Reyes E (2003) Molecular physiology of low-voltage-activated T-type calcium channels. Physiol Rev 83:117-161.

Rauner C, Köhr G (2011) Triheteromeric NR1/NR2A/NR2B receptors constitute the major N-methyl-D-aspartate receptor population in adult hippocampal synapses. J Biol Chem 286:7558-7566.

Schmidt-Hieber C, Jonas P, Bischofberger J (2004) Enhanced synaptic plasticity in newly generated granule cells of the adult hippocampus. Nature 429:184-187.

Steriade M (2006) Grouping of brain rhythms in corticothalamic systems. Neuroscience 137:1087-1106.

Talbot MJ, Sayer RJ (1996) Intracellular QX-314 inhibits calcium currents in hippocampal CA1 pyramidal neurons. J Neurophysiol 76:2120-2124.

Talley EM, Cribbs LL, Lee JH, Daud A, Perez-Reyes E, Bayliss DA (1999) Differential distribution of three members of a gene family encoding low voltage-activated (T-type) calcium channels. J Neurosci 19:1895-1911.

Thomas MJ, Watabe AM, Moody TD, Makhinson M, O'Dell TJ (1998) Postsynaptic complex spike bursting enables the induction of LTP by theta frequency synaptic stimulation. J Neurosci 18:7118-7126.

Wenzel A, Fritschy JM, Möhler H, Benke D (1997) NMDA receptor heterogeneity during postnatal development of the rat brain: differential expression of the NR2A, NR2B, and NR2C subunit proteins. J Neurochem 68:469-478.

Wisniewska MB, Misztal K, Michowski W, Szczot M, Purta E, Lesniak W, Klejman ME, Dabrowski M, Filipkowski RK, Nagalski A, Mozrzymas JW, Kuznicki J (2010) LEF1/β-catenin complex regulates transcription of the $Ca_V3.1$ calcium channel gene (*Cacna1g*) in thalamic neurons of the adult brain. J Neurosci 30:4957-4969.

Figure Legends

Figure 1. Thalamoreticular vs. corticoreticular inputs. ***A***, Scheme of a thalamocortical slice with recording electrode in the nRt and stimulating electrode in cortical layer 6. ***B***, Average EPSCs evoked by two stimuli (50 ms), showing either paired-pulse depression (black) or paired-pulse facilitation (gray). Inset, superimposition of the first peaks reveals different response latencies. ***C***, Plot of latency values vs. paired-pulse ratio (PPR), indicating that depressant responses (n = 9, black) display shorter latencies than facilitating responses (n = 8, gray; p = 0.01 between groups). Filled circles represent mean values. ***D***, Depressant inputs (PPD) display significantly larger amplitudes than facilitating inputs (PPF). *, $p < 0.05$.

Figure 2. GluN2B-NMDARs dominate at thalamoreticular synapses. ***A***, Thalamoreticular EPSCs in a cell voltage-clamped at -70 mV in control (black) and in the presence of 100 μM DL-APV (green). NMDAR blockade induced an increase in decay slope (bars; n = 9; $p < 0.01$). ***B***, NMDAR blockade did not affect EPSC peak and PPR (n = 9, $p > 0.05$). Inserted traces are average EPSCs in control and in DL-APV. ***C***, Top, examples of AMPAR- and NMDAR-mediated components at -70 mV and +40 mV, respectively. NMDA-EPSCs were isolated with 40 μM DNQX. Bottom, NMDA/AMPA ratio significantly decreased after 2 weeks (2 wk-old, n = 9; 3-4 wk-old, n = 14; 7-8 wk-old, n = 10, *, $p < 0.05$). ***D***, Top, overlay of scaled NMDA-EPSCs at different developmental stages, coded in gray scale. No change in decay kinetics occurred, as indicated by comparable values of weighted τ (τ_W) of bi-exponential fit (bars: 2 wk-old, n = 6; 3-4 wk-old, n = 16; 7-8 wk-old, n = 6). ***E***, Pharmacological profile of NMDA-EPSCs (2 wk-old, n = 6; 3-4 wk-old, n = 8; 7-8 wk-old, n = 6). Upper insets, example NMDA-EPSCs showing progressive reduction of control responses (black) after superfusion of NVP (red) and NVP+CP (blue). ***F***, Left, mean effects of GluN2-specific

blockers in 3-4 wk-old mice (NVP, n = 8; CP, n = 8; PPDA, n = 7). Right, example NMDA-EPSCs showing progressive reduction upon blocker superfusion, as indicated. ***G,H*** EPSCs in a cell voltage-clamped at -70 mV in control (black) and in the presence of 500 nM PPDA (***G***, green) or 10 μM CP (***H***, blue). GluN2C/D inhibition induced an increase in decay slope (bars; n = 8; $p < 0.05$), whereas GluN2B blockade had no effect (bars; n = 6; $p > 0.05$). *, $p < 0.05$, **, $p < 0.01$ drug vs. control.

Figure 3. GluN2B-NMDARs mediate thalamoreticular plasticity. ***A***,***B***, Time course of EPSCs at thalamoreticular synapses. Shadowed insets show pairing protocol applied after 10 min baseline. Low-threshold bursts were paired with synaptic stimulation (EPSP) for 3 min (***A,*** n = 7) or 6 min (***B,*** n = 7), which induced EPSC potentiation. Traces in the lower insets are average EPSCs evoked during baseline (1, gray) and during the last 10 min of recording (2, black). *, $p < 0.05$, **, $p < 0.01$ baseline vs. end of recording. ***C-F***, Same representation as in ***A***,***B***. Synaptic potentiation was not induced when EPSPs were omitted (***C***, n = 10), or not paired with bursts (***D***, n = 9). Pairing-induced plasticity was prevented by GluN2B-NMDAR blockade with CP (***E***, n = 9), but not by inhibition of GluN2A and GluN2C/D with NVP and PPDA (***F***, n = 10). ***G***, Potentiation was not accompanied by significant changes in PPR, as tested at the beginning of baseline (1) and at the end of the recording (2) in a subset of cells from ***A*** and ***B***. ***H***, Summary of data presented in ***A-F***. Short horizontal lines represent means from series with 3 min (white circles) and 6 min (gray circles) oscillations. Asterisks represent significant difference from the corresponding "no EPSP" series (one-way ANOVA on log-transformed values, followed by *post hoc* Student's t-test; *, $p < 0.05$, **, $p < 0.01$).

Figure 4. $Ca_V3.3$ channels are required for thalamoreticular plasticity. ***A***, Time course of EPSCs in nRt cells patched with a solution containing 0.5 mM QX-314 (n = 7). Shadowed insets show pairing

protocols applied after 10 min baseline, with examples of average EPSCs during baseline (1) and at the end of recording (2). During induction, low-threshold bursts were largely preserved, while action potentials were blocked, which resulted in significant potentiation (n = 7) ***B***, Same representation as in ***A***. Sinusoidal current injections were replaced by squared current pulses applied to nRt cell held -60 mV, to promote tonic firing over low-threshold bursting. No change in synaptic efficacy was induced (n = 8). ***C***,***D***, Same representation as in ***A***. Suppression of burst-induced Ca^{2+} with intracellular BAPTA (n = 6) and in $Ca_V3.3^{-/-}$ mice (n = 8) prevented potentiation. *, $p < 0.05$ baseline vs. end of recording.

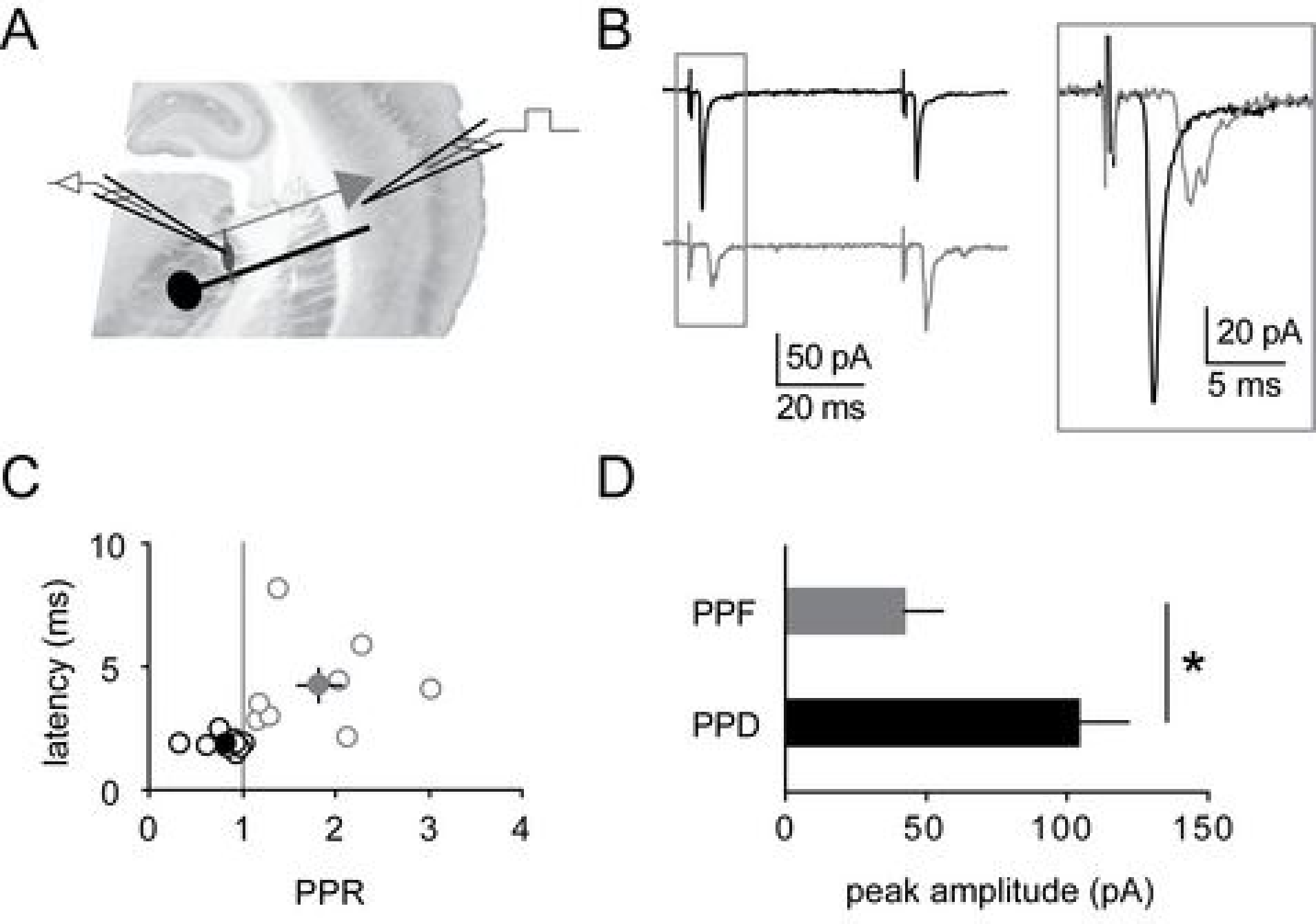
A
B
50 pA
20 ms
20 pA
5 ms
C
latency (ms)
10
5
0
0
1
2
3
4
PPR
D
PPF
PPD
*
0
50
100
150
peak amplitude (pA)

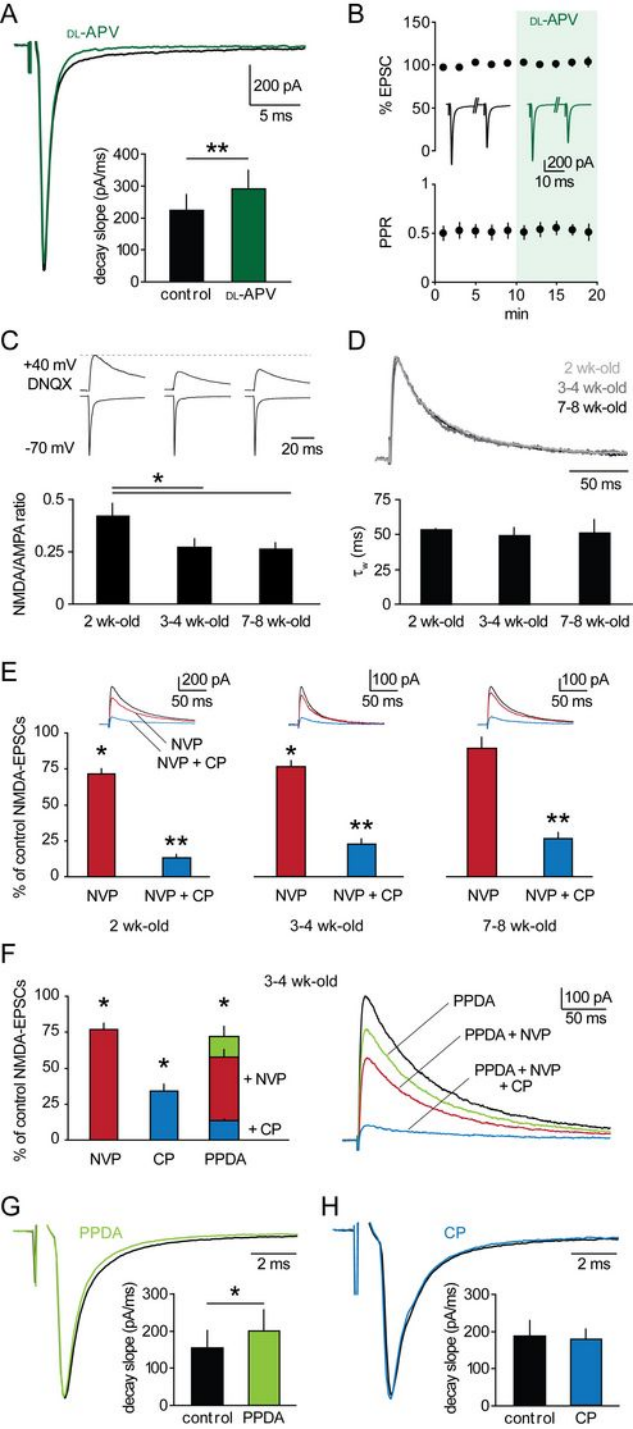
A
DL-APV
200 pA
5 ms
decay slope (pA/ms)
400
300
200
100
0
**
control
DL-APV
B
% EPSC
150
100
50
0
DL-APV
200 pA
10 ms
PPR
1
0.5
0
0
5
10
15
20
min
C
+40 mV
DNQX
-70 mV
20 ms
NMDA/AMPA ratio
0.5
0.25
0
*
2 wk-old
3-4 wk-old
7-8 wk-old
D
2 wk-old
3-4 wk-old
7-8 wk-old
50 ms
τw (ms)
75
50
25
0
2 wk-old
3-4 wk-old
7-8 wk-old
E
200 pA
50 ms
100 pA
50 ms
100 pA
50 ms
NVP
NVP + CP
% of control NMDA-EPSCs
100
75
50
25
0
*
**
NVP
NVP + CP
2 wk-old
3-4 wk-old
7-8 wk-old
F
3-4 wk-old
% of control NMDA-EPSCs
100
75
50
25
0
*
+ NVP
+ CP
NVP
CP
PPDA
PPDA
PPDA + NVP
PPDA + NVP
+ CP
100 pA
50 ms
G
PPDA
2 ms
decay slope (pA/ms)
300
200
100
0
*
control
PPDA
H
CP
2 ms
decay slope (pA/ms)
300
200
100
0
control
CP

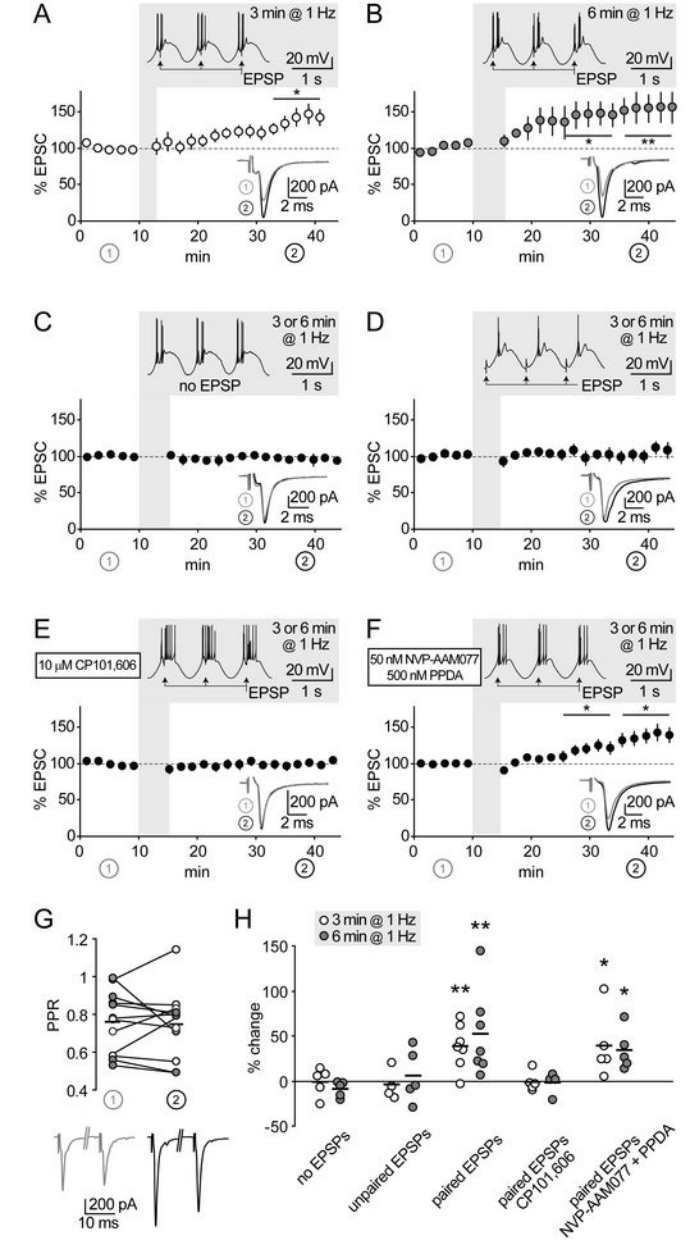
A
3 min @ 1 Hz
20 mV
EPSP
1 s
% EPSC
200 pA
2 ms
min
B
6 min @ 1 Hz
C
no EPSP
3 or 6 min @ 1 Hz
D
E
10 μM CP101,606
F
50 nM NVP-AAM077
500 nM PPDA
G
PPR
H
3 min @ 1 Hz
6 min @ 1 Hz
% change
no EPSPs
unpaired EPSPs
paired EPSPs
paired EPSPs CP101,606
paired EPSPs NVP-AAM077 + PPDA

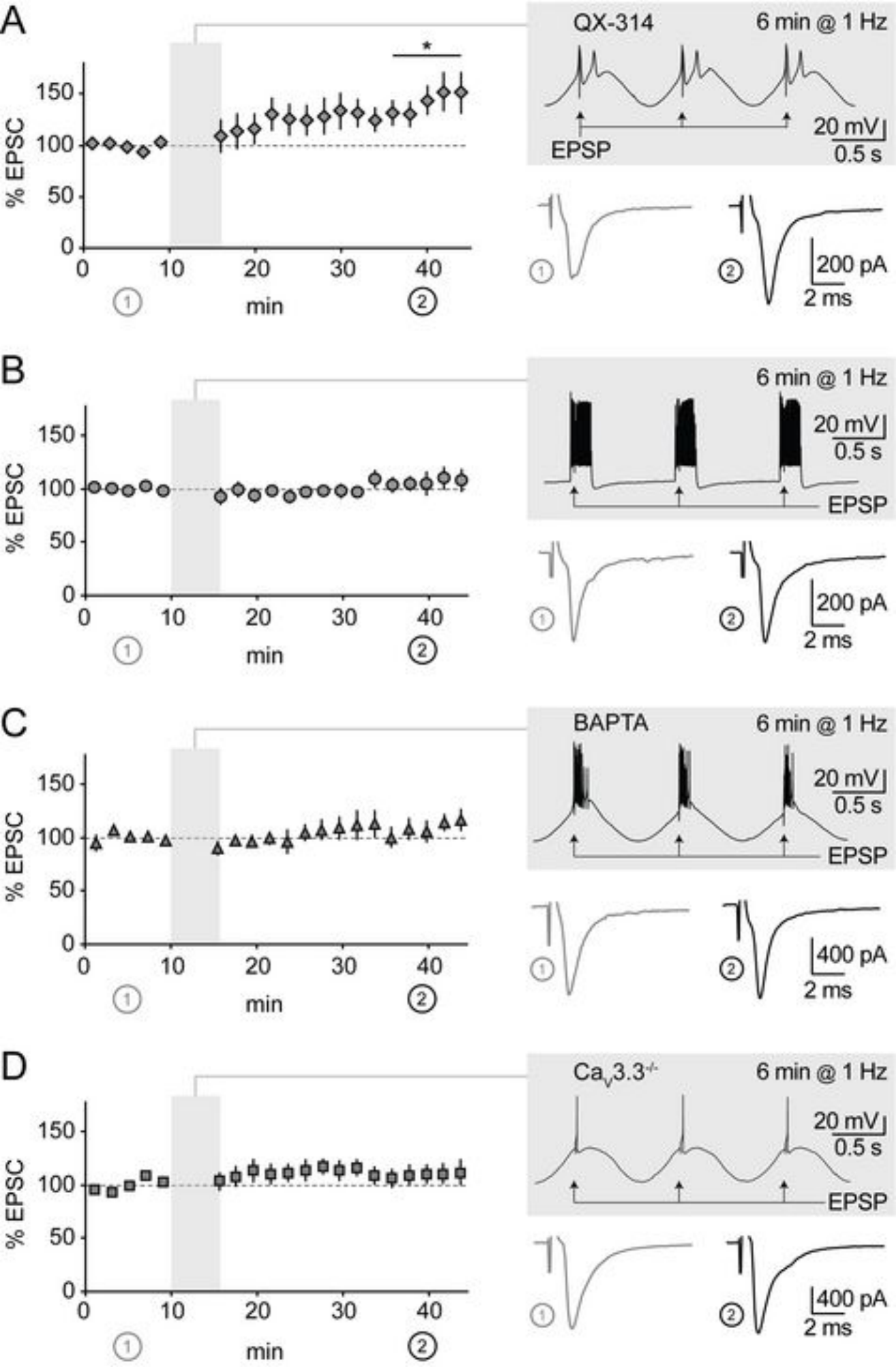
A
% EPSC
150
100
50
0
0
10
20
30
40
min
①
②
*
QX-314
6 min @ 1 Hz
20 mV
0.5 s
EPSP
200 pA
2 ms
B
% EPSC
150
100
50
0
0
10
20
30
40
min
①
②
6 min @ 1 Hz
20 mV
0.5 s
EPSP
200 pA
2 ms
C
% EPSC
150
100
50
0
0
10
20
30
40
min
①
②
BAPTA
6 min @ 1 Hz
20 mV
0.5 s
EPSP
400 pA
2 ms
D
% EPSC
150
100
50
0
0
10
20
30
40
min
①
②
Cav3.3-/-
6 min @ 1 Hz
20 mV
0.5 s
EPSP
400 pA
2 ms